2-1-2021

The Zebrafish Visual System Transmits Dimming Information via Multiple Segregated Pathways

Estuardo Robles
Purdue University, erobles@smith.edu

Nicholas P. Fields
Purdue University

Herwig Baier
Max-Planck-Institut für Neurobiologie

Received: 9 September 2019 | Revised: 20 May 2020 | Accepted: 21 May 2020

DOI: 10.1002/cne.24964

RESEARCH ARTICLE

JCN RESEARCH IN SYSTEMS NEUROSCIENCE THE JOURNAL OF COMPARATIVE NEUROLOGY WILEY

The zebrafish visual system transmits dimming information via multiple segregated pathways

Estuardo Robles[1] | Nicholas P. Fields[1] | Herwig Baier[2]

[1]Department of Biological Sciences and Purdue Institute for Integrative Neuroscience, Purdue University, West Lafayette, Indiana

[2]Max Planck Institute for Neurobiology, Martinsried, Germany

Correspondence
Estuardo Robles, Department of Biological Sciences and Purdue Institute for Integrative Neuroscience, Purdue University, West Lafayette, IN 47907.
Email: roblese@purdue.edu

Funding information
Max-Planck-Gesellschaft; Purdue Institute for Integrative Neuroscience

Abstract

Vertebrate retinas contain circuits specialized to encode light level decrements. This information is transmitted to the brain by dimming-sensitive OFF retinal ganglion cells (OFF-RGCs) that respond to light decrements with increased firing. It is known that OFF-RGCs with distinct photosensitivity profiles form parallel visual channels to the vertebrate brain, yet how these channels are processed by first- and higher order brain areas has not been well characterized in any species. To address this question in the larval zebrafish visual system, we examined the visual response properties of a genetically identified population of tectal neurons with a defined axonal projection to a second-order visual area: *id2b*:*gal4*-positive torus longitudinalis projection neurons (TLPNs). TLPNs responded consistently to whole-field dimming stimuli and exhibited the strongest responses when dimming was preceded by low light levels. Functional characterization of OFF-RGC terminals in tectum revealed responses that varied in their photosensitivities: (a) low-sensitivity OFF-RGCs that selectively respond to large light decrements, (b) high-sensitivity OFF-RGCs that selectively encode small decrements, and (c) broad sensitivity OFF-RGCs that respond to a wide range of light decrements. Diverse photosensitivity profiles were also observed using pan-neuronal calcium imaging to identify dimming-responsive neurons in both tectum and torus longitudinalis. Together, these data support a model in which parallel OFF channels generated in the retina remain segregated across three stages of visual processing. Segregated OFF channels with different sensitivities may allow specific aspects of dimming-evoked behaviors to be modulated by ambient light levels.

KEYWORDS

dimming, functional imaging, larval visual motor response, multiphoton, OFF pathway, *RRID*:*ZFIN_ZDB-ALT-090116-2*, *RRID:ZFIN_ZDB-ALT-090715-16*, *RRID:ZFIN_ZDB-GENO-140811-5*

1 | INTRODUCTION

Vertebrate retinas dedicate a large proportion of cells and synapses to the processing of dark information, likely reflecting an evolutionary adaptation driven by the abundance of dark regions in natural scenes (Ratliff, Borghuis, Kao, Sterling, & Balasubramanian, 2010). Light decrement information is transmitted to the brain primarily via OFF

Abbreviations: BS, broad sensitivity; DLR, dorsal light reflex; GUI, graphical user interface; HS, high sensitivity; LS, low sensitivity; RGC, retinal ganglion cell; ROI, region of interest; SAC, stratum album centrale; SFGS, stratum fiibrosum et griseum superficiale; SGC, stratum griseum centrale; SM, stratum marginale; SO, stratum opticum; SPV, stratum periventriculare; TLPN, torus longitudinalis projection neuron; TL, torus longitudinalis.

retinal ganglion cells (OFF-RGCs), which respond to light decrements with increased firing. In the mammalian retina, interneuron circuits downstream of rod and cone photoreceptors generate OFF-RGC pathways with distinct photosensitivity thresholds (Völgyi, Deans, Paul, & Bloomfield, 2004). While the adult zebrafish retina contains the vertebrate-typical complement of both high-sensitivity (HS) rod photoreceptors and low-sensitivity (LS) cone photoreceptors (Fleisch & Neuhauss, 2006), electroretinogram recordings have shown that rod responses contribute little to the larval retina's photosensitivity before 15 dpf (Bilotta, Saszik, & Sutherland, 2001). However, it is clear that the cone-dominated larval retina supports an extensive repertoire of visual behaviors across a wide range of light levels, including responses to whole-field motion, prey capture, and escape from a looming predator (Portugues & Engert, 2009). Defining how the zebrafish visual system responds to varying light levels is essential for building a more complete understanding of their sensory ecology. However, it is unknown whether small and large light decrements are processed by distinct visual circuits.

Several studies have demonstrated the presence of both direction-selective (Gabriel, Trivedi, Maurer, Ryu, & Bollmann, 2012; Kramer, Wu, Baier, & Kubo, 2019; Nikolaou et al., 2012) and orientation-selective RGC inputs (Antinucci, Suleyman, Monfries, & Hindges, 2016) to the larval zebrafish optic tectum. In addition, experimental evidence has also been provided that subsets of zebrafish RGCs are tuned to detect ecologically relevant visual stimuli such as prey (Semmelhack et al., 2014) and looming stimuli (Temizer, Donovan, Baier, & Semmelhack, 2015). We previously demonstrated that specific tectal sublayers contained a large proportion of OFF-responsive RGCs (Robles, Filosa, & Baier, 2013). However, it is unknown if OFF-RGCs in the larval zebrafish are subdivided into functional types with different photosensitivity thresholds. If these exist, do they remain segregated in OT or do they converge to confer broad photosensitivity profiles to OFF circuits in the tectum? Torus longitudinalis (TL) is a non-retinorecipient higher order visual area that has been shown to contain dimming-sensitive neurons (Northmore, 2017). Does it contain dimming neurons with different photosensitivities? If so, are there dedicated, genetically specified projections from tectum to TL that selectively transmit different types of light decrement information?

In this study, we utilized genetically targeted functional imaging to determine if the larval zebrafish brain contains visual circuits specialized to process light decrements of different amplitudes. Genetically targeted functional calcium imaging of *id2b:gal4*-positive torus longitudinalis projection neurons (TLPNs) revealed responses to whole-field dimming stimuli that were specifically tuned to small decrements (light decrements preceded by low light levels). Calcium imaging of RGC axon terminals in the optic tectum confirmed the presence of OFF-RGC inputs with a wide range of photosensitivity profiles in response to broad-spectrum dimming stimuli. These generally consisted of three response classes: (a) LS OFF-RGCs that responded best to large decrements, (b) HS OFF-RGCs that responded best to small decrements, and (c) broad sensitivity (BS) OFF-RGCs that responded similarly to both small and large decrements. Identification of HS OFF-RGCs selective for small light decrements suggests that wiring specificity between this class of OFF-RGCs and dendrites of TLPNs confers them with their HS dimming responses. Consistent with this model, HS OFF-RGCs preferentially innervate layers of tectal neuropil targeted by TLPN dendrites. Functional imaging also identified dimming-responsive neurons with diverse photosensitivity profiles in both optic tectum and TL. These findings suggest that visual pathways that transmit dimming information regarding both small and large light decrements remain segregated across three levels of processing: retina, tectum, and TL. Together, these findings support a model in which segregated visual pathways for dimming information may support contextual modulation of dimming evoked behaviors by the ambient light level.

2 | METHODS

2.1 | Fish lines

All animal procedures conformed to the institutional guidelines set by EU, Germany, and local government authorities (Regierung von Oberbayern) and the Purdue University Institutional Animal Care and Use Committee (IACUC). Zebrafish adults and larvae were maintained at 28°C on a 14/10 h light/dark cycle. Previously described transgenic lines used in this study: *Tg(atoh7:gal4) RRID:ZFIN_ZDB-ALT-090715-16*, *Tg(Elavl3:gal4) RRID:ZFIN_ZDB-ALT-090116-2*, *Tg(14xuas:gcamp6s) RRID:ZFIN_ZDB-GENO-140811-5*, *Tg(elavl3:LY-TagRFP)*, *and Tg(id2b:gal4)*. All larvae used were mutants for *mitfa*$^{-/-}$ *(nacre)*.

2.2 | Embryo injections

Genetic mosaic labeling of single neurons by expression of a membrane-targeted tdTomato was achieved by injection of the 4xnrUAS:tdTomato-caax plasmid (a gift from B. Appel and J. Hines, University of Colorado, Denver, CO), along with RNA encoding Tol2 transposase into *Tg(id2b:Gal4-VP16)* × *Tg(uas:gcamp6s)* double transgenic embryos. DNA construct was pressure-injected at a concentration of 25–50 ng/L into one- to eight-cell-stage embryos.

2.3 | Multiphoton imaging

For live imaging, 6–7 dpf larvae were embedded in 2% low-melting-point agarose. GCaMP6s imaging was performed as described previously (Robles, Laurell, & Baier, 2014). For cell type-specific functional imaging in Figure 1 TLPNs were identified by one of two methods: (a) sparse tdTomato-caax labeling or (b) morphological identification of neuronal cell bodies with a medially directed axonal projection in *Tg(id2b:gal4)* × *Tg(uas:gcamp6s)* larvae. 7 dpf *Tg(14xUAS-GCAMP6S) nacre* larvae were imaged with a custom-built two-photon microscope equipped with a mode-locked Ti:Sapphire Chameleon UltraII laser (Coherent) tuned to 920 nm and controlled by the ScanImage v3.6 software (Pologruto, Sabatini, & Svoboda, 2003). Time series were acquired with a 40× water-immersion objective (Zeiss, NA 0.8) at a

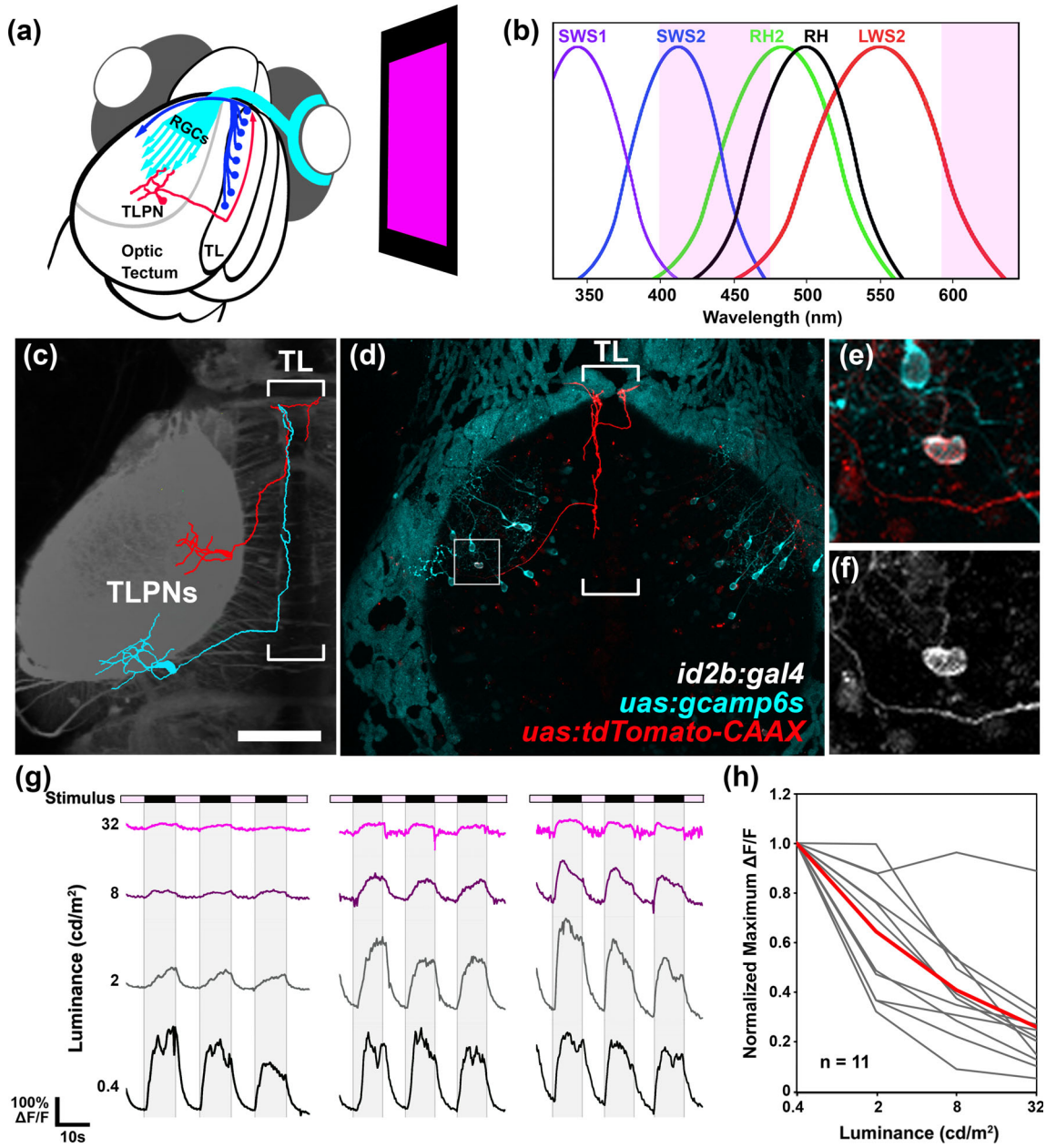

FIGURE 1 Torus longitudinalis projection neuron (TLPN) responses to whole-field dimming stimuli. (a) Schematic overview of experiments performed in this study. An organic light-emitting diode (OLED) screen equipped with magenta filters is positioned in front of one eye of an agarose-embedded *Tg(id2b:gal4,uas:gcamp6s)* double transgenic larva, which drives tissue-specific expression of the calcium sensor protein GCaMP6s. (b) Absorption curves for the photopigments expressed in UV cones (SWS1), blue cones (SWS2), green cones (RH2), red cones (LWS2), and rods (RH1). Region shaded in magenta indicates the wavelength range generated by the OLED stimulus, simultaneously activating rods as well as red, green, and blue cones. (c) Skeletonized tracings of two TLPNs overlayed on a gray scale dorsal view image of Tg(*elavl3:LY-TagRFP)* brain containing left tectum and TL. Note that posterior positioned TLPN innervates TL posteriorly, whereas anteriorly positioned TLPN enters TL at its anterior pole and crosses the midline to innervate contralateral TL. (d) Dorsal view of a 7 dpf *Tg(id2b:gal4,uas:gcamp6s)* larva that was pressure injected at the early embryo stage to yield sparse tdTomato:CAAX labeling within the *id2b:gal4* expression pattern. Note sparse tdTomato labeling of a single tectal neuron with an axon that enters TL, extends anteriorly, and crosses the midline within TL. (e) Higher magnification view of boxed regions in (d). (f) GCaMP6s fluorescence of TLPN cell body within boxed region in (d). (g) Example traces of GCaMP6s fluorescence from three individual TLPN neurons during presentation of whole-field dimming stimuli with the following ON light intensities: 0.4, 2, 8, and 32 cd/m^2. All three TLPNs responded maximally to trials with low intensity stimuli (≤2 cd/m^2). (h) Effect of stimulus intensity on maximum ΔF/F values during OFF phase for 11 TLPNs during presentation of trials at the following light intensities: 0.4, 2, 8, and 32 cd/m^2. Data from individual trials are shown in gray. Average of the 11 individual traces is shown in red. Scale bar: 100 μm in (a), 30 μm in (b)

rate of 3.6 Hz and 0.4 × 0.4 μm resolution. Ambient light levels were approximately 0.05 cd/m^2 during recording and dark adaptation (30 min prior to experiment and 3 min between trials). Visual stimulus was generated with the Vision Egg software (Straw, 2008) and presented monocularly with an 800 × 600 pixel organic light-emitting diode (OLED, eMagin, USA) with a magenta Wratten filter (Kodak #32) used to block green light between 520 and 580 nm. Filtering was necessary to minimize contamination of the fluorescence detection pathway with stimulus illumination. The screen was positioned 1 cm away from the larvae and spanned approximately 60° of the visual field. The light intensities used (0.4, 2, 8, and 32 cd/m^2) correspond to Weber contrasts of 7, 39, 159, and 639. Bright photopic stimulation was not possible during multiphoton imaging due to interference with GCaMP6s fluorescence detection.

2.4 | Data analysis

Motion artifacts from time-lapse recordings were removed using the TurboReg plugin in ImageJ/FIJI. Subsequent imaging trials conducted on the same fish and same image plane were combined (concatenated) to streamline image segmentation workflow. Automatic segmentation of regions of interest (ROIs) based on fluorescence activity of pixel clusters was performed using the CalciumSignalExtract graphical user interface (GUI) for Matlab (Mathworks) written by Meyer Zum Alten Borgloh (2015). Active neurons were selected by specifying a threshold value of 0.7 for the segmentation, thereby ensuring that pixels were only included in ROI segmentation if they reached an intensity 70% above baseline. ROI data series generated by CalciumSignalExtract GUI were used to run K-means clustering algorithm in Matlab (using "correlation" distance metric) and generate silhouette plots. For photosensitivity threshold assessment, OFF ROIs were classified as LS if the maximum ΔF/F values measured during the OFF phase of trials with a prestimulus light intensity of 32 cd/m^2 were at least twofold greater than the maximum value measured during trials at 0.4 cd/m^2. Neurons were classified as HS if maximum ΔF/F during the OFF phase of trials at 0.4 or 2 cd/m^2 were at least twofold greater than during trials at 32 cd/m^2. Neurons were classified as BS if maximum ΔF/F during the OFF phase did not change more than 1.9-fold compared to trials with a prestimulus light level of 0.4 cd/m^2. For Elavl3 imaging experiments, analysis was restricted to detected ROIs with consistent responses at each stimulus presentation to exclude neurons that were active during trials but lacked consistent stimulus-locked responses. These excluded neurons may represent neuronal elements within spontaneously active ensembles previously described in the larval zebrafish tectum (Pérez-Schuster et al., 2016). ROI color designations were manually reassigned to match functional classifications using Adobe Photoshop.

2.5 | Statistical analysis

Data sets were analyzed using the GraphPad Prism software version 801 (GraphPad Software, Inc., La Jolla, CA). One-way analysis of variance (ANOVA) was used to identify differences among means for data sets with three or more groups. *p*-values less than .05 were considered significant. If a significant difference was detected with the ANOVA, Dunnett's test was used for specific comparisons to a control. Graph in Figure 6 shows mean ± standard error of the mean.

3 | RESULTS

3.1 | TLPNs respond to whole-field dimming stimuli

To functionally characterize TLPN responses, we performed in vivo two-photon calcium imaging using double transgenic larvae in which the calcium sensor GCaMP6s is expressed under the control of the *id2b:gal4* BAC transgene (DeMarco, Xu, Baier, & Robles, 2019): *Tg(id2b:gal4) × Tg(UAS:GCaMP6s)*. Visual stimuli were presented to a single eye via an OLED screen equipped with magenta filters to minimize interference with GCaMP6s fluorescence detection (Figure 1a,b). The stimulus was designed to deliver a broad spectrum of light capable of efficiently stimulating rods as well as blue, green, and red cones (UV cones were not strongly stimulated by this display). Preliminary trials confirmed that a full-screen alternating stimulus (7-s stimulus-ON/10-s stimulus-OFF) evoked strong and consistent responses in tectum (data not shown). We have previously identified a neuron type labeled by an *id2b:gal4* transgene that forms a topographic projection from tectum to TL (Figure 1c; DeMarco et al., 2019). Although multiple tectal neuron types are labeled by *id2b:gal4*, the TLPN is the only type with a dendrite targeting SGC and SFGS5/6 layers of tectum and an axon that extends medially en route to TL. These morphological features allowed positive identification of TLPN cell bodies in *Tg(id2b:gal4) × Tg(uas:gcamp6s)* larvae (Figure 1d-f).

Preliminary trials using moving spot stimuli revealed weak responses to small moving spots (1–5°, 30°/s, positive contrast) and stronger responses to large spots (20–40°, 30°/s, positive contrast). Closer examination revealed that TLPN responses coincided with the disappearance of the large spot from the screen, which led us to identify whole-field light steps as the optimal stimuli for TLPNs (data not shown). As shown in Figure 1g (lower traces), TLPN OFF responses to whole-field light decrements consisted of a large increase in GCaMP6s fluorescence that was sustained during the 10-s long OFF phase of the stimulus. To determine if TLPNs are tuned to large or small light decrements, we presented a full-screen dimming stimulus (7-s stimulus-ON/10-s stimulus-OFF) while varying the light level during the ON phase of the stimulus (ON light level was increased from 0.4–2 to 8–32 cd/m^2 in subsequent trials, all of which are ecologically relevant light intensities; Cook & McReynolds, 1998). Presentation of this dimming stimulus series confirmed that TLPNs are dimming responsive. Moreover, the majority of recorded TLPNs (10 of 11) were maximally responsive to the lowest intensity stimulus (0.4 cd/m^2 during ON) and exhibited only weak responses to the largest light decrement tested (32 cd/m^2; Figure 1g). It should be noted that the tuning of TLPN dimming responses exhibited a high degree of

variability, with a range of response strengths at intermediate ON light intensities (2 and 8 cd/m^2; Figure 1h). These findings indicate that dimming information is transmitted from tectum to TL by TLPNs, and a majority of *id2b:gal4*-positive TLPNs are specialized to transmit information regarding small light decrements.

3.2 | OFF-RGC inputs to tectum exhibit a range of photosensitivity profiles

Based on the dimming responses in TLPNs, we sought to determine whether the tectum is innervated by OFF-RGCs with a preference for small light decrements. The absence of such RGC responses would suggest that the photosensitivity of TLPNs is an emergent property of tectal circuitry. We performed functional imaging in RGC axons using larvae in which GCaMP6s is expressed under the control of an RGC-specific transgene (*Tg(atoh7:gal4)* × *Tg(UAS:GCaMP6s)*; Figure 2a). To identify RGC axon terminals based on their stimulus-evoked responses, we utilized a cross-correlation-based image segmentation approach to identify pixel clusters with identical temporal dynamics (see Section 2 and Meyer Zum Alten Borgloh, 2015). Each ROI identified in this manner corresponds to either the cross-section of an individual RGC axon terminal or multiple closely apposed terminals with identical response kinetics (Figure 2b). To objectively classify ROIs based on their functional responses, we initially performed *k*-means clustering on ROI time series data using a *k* value of 3 based on the prediction that we would detect OFF, ON, and ON–OFF RGC terminals. This preliminary analysis did separate ROIs into groups with visibly different response profiles (Figure 2c). In particular, one cluster contained exclusively ROIs with strong OFF responses that varied in the duration of their response (Figure 2d).

To determine if a *k* value of 3 is optimal for RGC responses obtained using this whole-field stimulus, we performed *k*-means clustering on a larger ROI time series data set (325 ROIs from 10 larvae) specifying *k* values from 2 to 4. Figure 3a,b displays raster plots of the clustering results for $k = 2$ and $k = 3$. Note that OFF-RGCs (activated at light offset) were similarly grouped into Cluster 1 in both cases (93% identical). In order to determine which *k* value most accurately clustered the data, we generated silhouette plots, where the silhouette value reflects how similar a trace is to its own cluster compared to other clusters. Silhouette analysis revealed that the data were best fit by $k = 2$, as evidenced by the higher average silhouette value (0.679) compared to *k* values of 3 and 4 (0.514 and 0.435, respectively; Figure 3c-e). This suggests a lack of clear separation between putative ON RGCs and ON–OFF RGCs across larvae. This is likely due to the fact that a large proportion of cells with ON responses had transient OFF responses that were largely variable in both amplitude and duration. One potential explanation for this result is that ON-RGCs were not strongly activated by this visual stimulus due to having receptive fields with strong inhibitory surround suppression (Cook & McReynolds, 1998). Regardless, these findings confirm the presence of OFF-RGC axon terminals in the tectum that respond strongly to our whole-field dimming stimulus.

The photosensitivity profile of individual OFF-RGC axon terminals was determined by using the segmentation/classification workflow described above on sets of recordings obtained while varying display brightness during the ON phase of the stimulus. Display brightness during the ON phase was increased in subsequent trials from 0.4–2 to 8–32 cd/m^2. Automated ROI detection was performed on image stacks containing four trials at different light intensities acquired at the same plane of tectum. Figure 4a shows one tectal plane containing 47 ROIs classified as OFF-RGCs (magenta) at a light intensity of 32 cd/m^2. Subsequent ROI detection on trials using the low intensity stimulus (0.4 cd/m^2) identified a partially overlapping set of 36 ROIs (blue labeled ROIs in Figure 4b). More detailed analysis of ROIs detected at both 32 and 0.4 cd/m^2 revealed that they also exhibited strong responses at both intermediate light levels (Figure 4c, left panel). This response type was termed BS. Examination of ROIs activated at an ON light intensity of 0.4 cd/m^2 and not at 32 cd/m^2 revealed OFF-RGCs that responded most strongly at lower light levels (0.4 or 2 cd/m^2). This response type was termed HS (Figure 4c, right panel). Conversely, a subset of OFF-RGC ROIs were identified that responded more strongly to large light decrements (Figure 4c, middle panel), and this response type was termed LS. Overall, BS, LS, and HS OFF-RGC response types were present in every larva examined and occurred in similar proportions (25.5 ± 4.7%, 35.6 ± 4.7%, and 39 ± 5.1%, $p > .1$; data from 290 ROIs detected in eight larvae). It should be noted that within each of these categories, individual ROI responses did exhibit variability (see Figure 4d). However, all LS terminals responded most strongly to an ON phase with an intensity of 32 cd/m^2, and all HS terminals responded most strongly to an ON phase of either 2 or 0.4 cd/m^2 (Figure 5a-c). Therefore, it is likely that this functional diversity represents a spectrum of OFF-RGC photosensitivities consisting of multiple distinct types. Such diversity has previously been reported in larval zebrafish bipolar cells, which are presynaptic to RGCs (Odermatt, Nikolaev, & Lagnado, 2012). However, LS and HS categories clearly represent extremes along the spectrum of RGC OFF-responses. These findings suggest that HS dimming responses in *id2b:gal4*-positive TLPNs primarily reflect synaptic input from the HS class of OFF-RGCs.

3.3 | OFF-RGCs are routed to specific layers of the tectum

The existence of OFF-RGCs tuned to different size light decrements suggests that these parallel pathways may activate distinct visual circuits in the brain. The larval zebrafish tectum contains a multilayered neuropil, in which RGC axons innervate nine distinct tectal layers (Nikolaou et al., 2012; Robles et al., 2013; Robles, Laurell, & Baier, 2014; Xiao et al., 2011; Xiao & Baier, 2007). This precision is matched by retinorecipient neurons in the tectum, many of which form dendritic arbors that also stratify in specific tectal neuropil layers (Del Bene et al., 2010; Gabriel et al., 2012; Robles, Smith, & Baier, 2011; Scott & Baier, 2009). To determine if OFF-RGC functional classes preferentially innervate distinct layers of the tectal

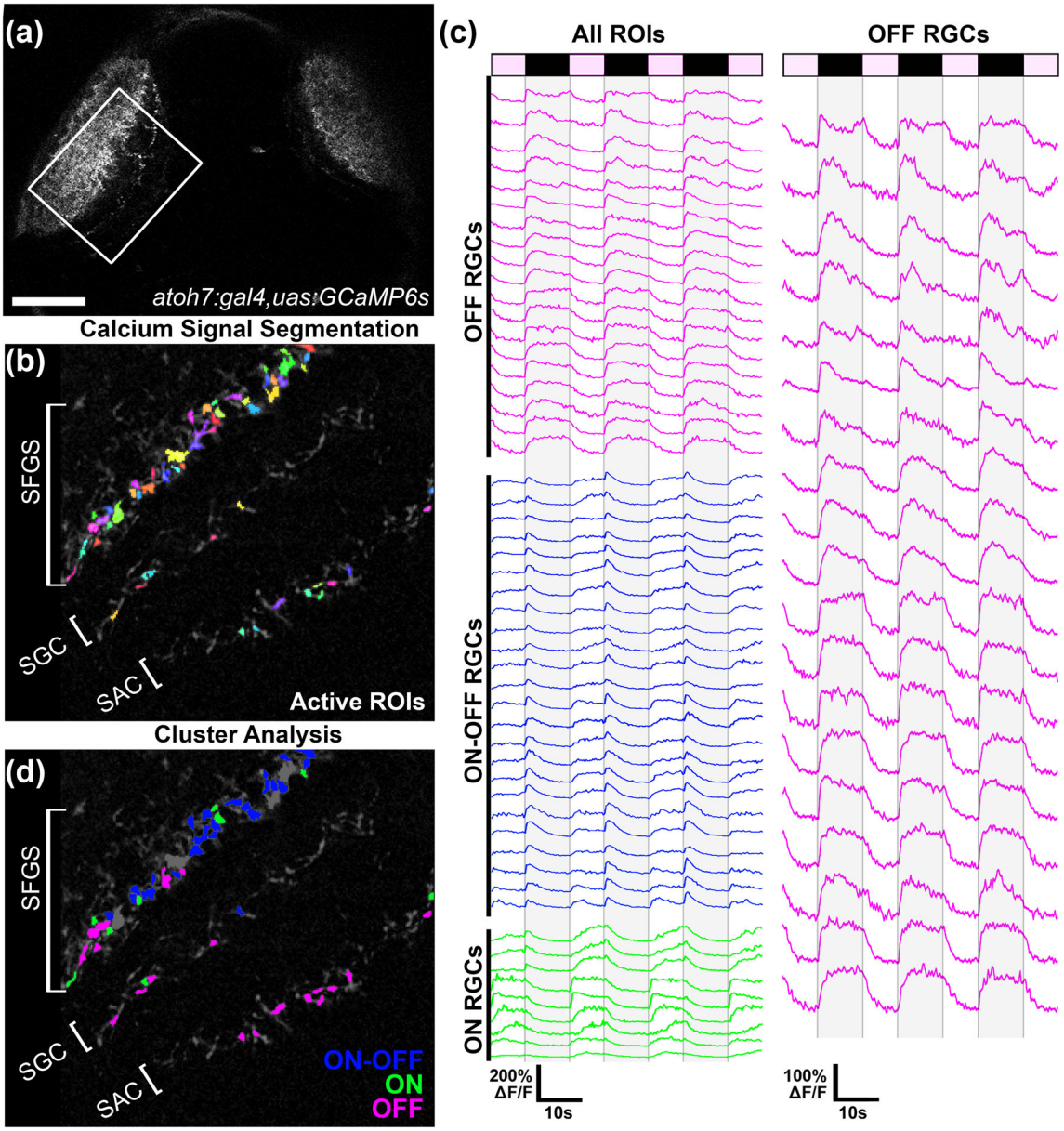

FIGURE 2 Functional identification of OFF retinal ganglion cell (OFF-RGC) terminals in vivo. (a) Low-magnification dorsal view of a 6 dpf *Tg (atoh7:gal4,uas:gcamp6s)* larva. Boxed region indicates typical field of view used for functional imaging trials. (b) Average intensity projection from a recording in the left tectum of a *Tg(atoh7:gal4,uas:gcamp6s)* larva presented with dimming stimuli to the right eye. Active regions of interest (ROIs) identified by cross-correlation-based image segmentation are displayed in different colors. Note multiple active regions in the SAC/SPV, SGC, and deepest sublayers of SFGS. (c) Fluorescence intensity traces of ROIs indicated in C during repeated presentation of dimming steps to the contralateral eye as indicated by light and dark bars at top. Each trace is 58 s in duration and consists of ON phases of 7-s duration and OFF phases of 10-s duration. Gray shading overlaid on traces indicates dimming phase when stimulus display is OFF. *k*-means cluster analysis divided ROIs into three groups based on their temporal dynamics, indicated by color coding in blue, green, and magenta. Magenta-colored traces represent dimming detector RGCs that exhibited strong and consistent OFF responses. (d) Average intensity projection shown in (b) presented with OFF ROI color coding that corresponds to clustering results shown in (c). Note that in this larva OFF-RGCs ROIs are located in the SAC/SPV, SGC, and deepest sublayers of SFGS (5/6). Data are from 52 ROIs detected in a single larva. Scale bar: 50 μm in (a), 20 μm in (b,d). SAC, stratum album centrale; SFGS, stratum fiibrosum et griseum superficiale; SGC, stratum griseum centrale; SPV, stratum periventriculare

neuropil, 290 OFF-RGC ROIs were identified in eight tecta, and individual ROIs were assigned to one of six retinorecipient sublayers: three subregions of the stratum fibrosum griseum superficiale (SFGS1/2, SFGS3/4, and SFGS5/6), the stratum opticum (SO), the stratum griseum centrale (SGC), or a thin layer at the boundary of the stratum album centrale and stratum periventriculare (SAC/SPV; Figure 6a). Overall, the majority of OFF-RGC terminals were located within the deepest SFGS layer,

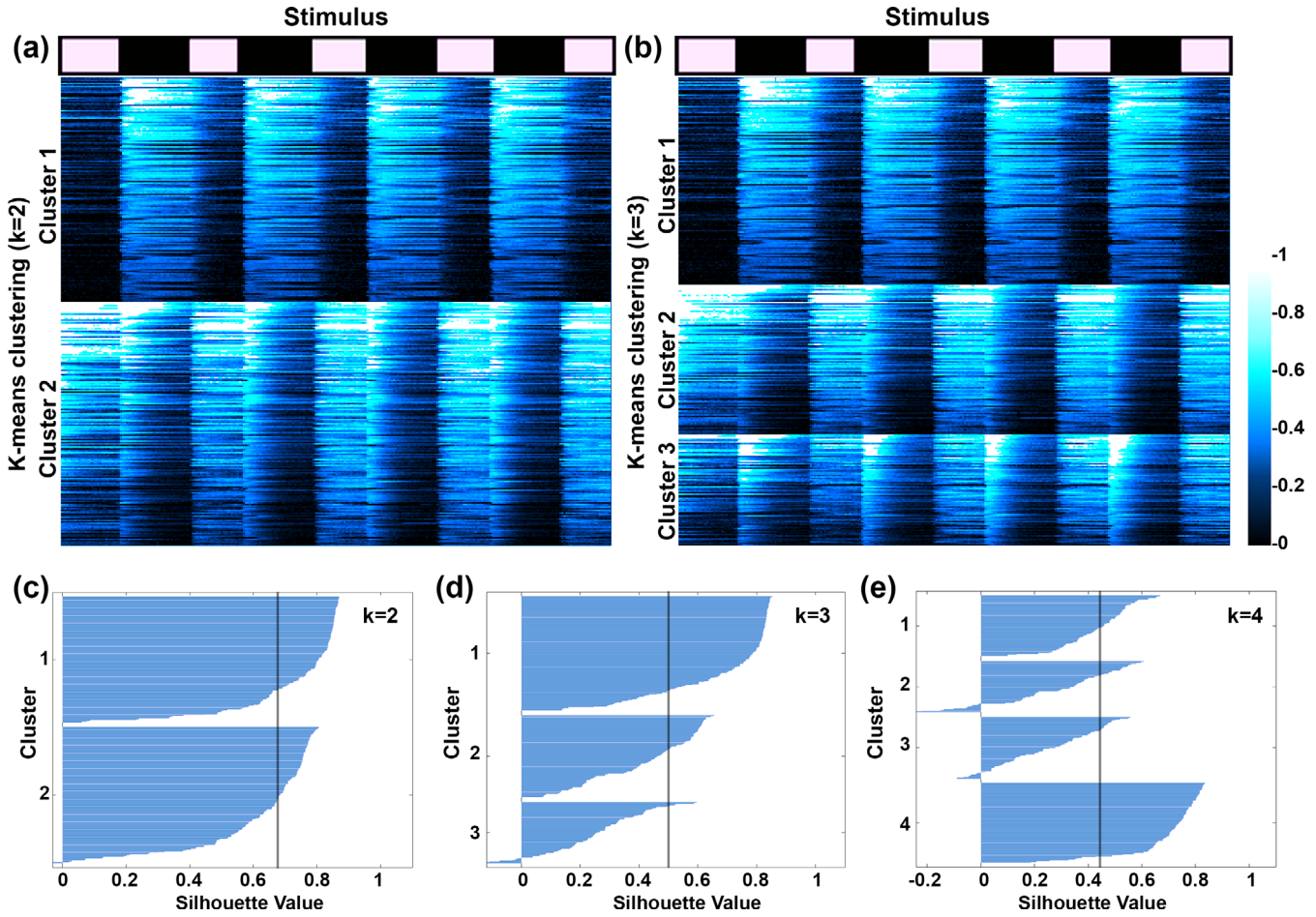

FIGURE 3 K-means clustering of automatically segmented retinal ganglion cell (RGC) regions of interest (ROIs). (a,b) Results of *ks*-means clustering for 325 individual ROIs from 10 *Tg(atoh7:gal4,uas:gcamp6s)* tecta using *k* values of 2 and 3. Stimulus timing is indicated at top, with total recording duration of 75 s (7-s stimulus-ON, 10-s stimulus-OFF). Fluorescence intensity for each recording is displayed as a color raster plot based on color scale at right. Note that in both (a and b), Cluster 1 is comprised of RGC terminals with strong and consistent OFF responses. (c–e) Silhouette plots for *k* values of 2, 3, and 4. Vertical gray line in each plot indicates average silhouette value. The highest average silhouette value in (c) indicates that the data are best fit by a *k* value of 2

SFGS5/6 (Figure 6b). Smaller fractions of OFF-RGCs were also located in SFGS3/4 and SGC. In contrast, SAC/SPV and SFGS1/2 were only very sparsely targeted by OFF-RGC terminals, and no OFF-RGC inputs were detected in SO. To confirm that these differences are not due to denser retinal innervation of specific sublayers, we compared the OFF-RGC distribution relative to projectome data that quantified the percentage of retinal inputs that terminate in each tectal layer (Robles et al., 2014). This analysis confirmed that overrepresentation of OFF-RGC terminals in SFGS5/6 is not simply due to denser RGC innervation. SFGS5/6 and SFGS3/4 receive similar fractions of all RGC inputs (30.2% vs. 25.6% of 446 axonal reconstructions), whereas we find SFGS5/6 to contain fourfold more OFF-RGC terminals than SFGS3/4 (62 ± 6.2% vs 14.3. ± 4.8%, p = .017, n of 8 tecta). Together, these findings show that OFF-RGC inputs are preferentially routed to SFGS5/6 and are also enriched in SFGS3/4 and SGC. In contrast, the deepest (SAC/SPV) and most superficial (SO and SFGS1/2) layers of the tectum are largely devoid of OFF-RGC inputs.

To determine if BS, HS, and LS OFF-RGC response types differ in their relative innervation of specific tectal layers, we examined the response type (LS/HS/BS) distribution of OFF-RGC ROIs in each tectal neuropil layer. In SFGS5/6, the tectal sublayer that receives a majority of OFF-RGC inputs, BS, HS, and LS inputs were present in roughly equal proportions (Figure 6b). Specific targeting of tectal sublayers was detected in SFGS3/4 and SAC/SPV. SFGS3/4 sublayers received a significantly higher proportion of HS OFF-RGC inputs compared to LS OFF-RGC inputs (62 ± 6.2% vs 14.3. ± 4.8%, p = .017, n of 8 tecta). In contrast, the SAC/SPV layer received a significantly higher proportion of LS OFF-RGC inputs compared to HS OFF-RGC inputs. Although not statistically significant, there was also a trend in the SGC toward preferential innervation by BS and HS OFF-RGCs. Given that many retinorecipient neurons in the tectum form dendritic

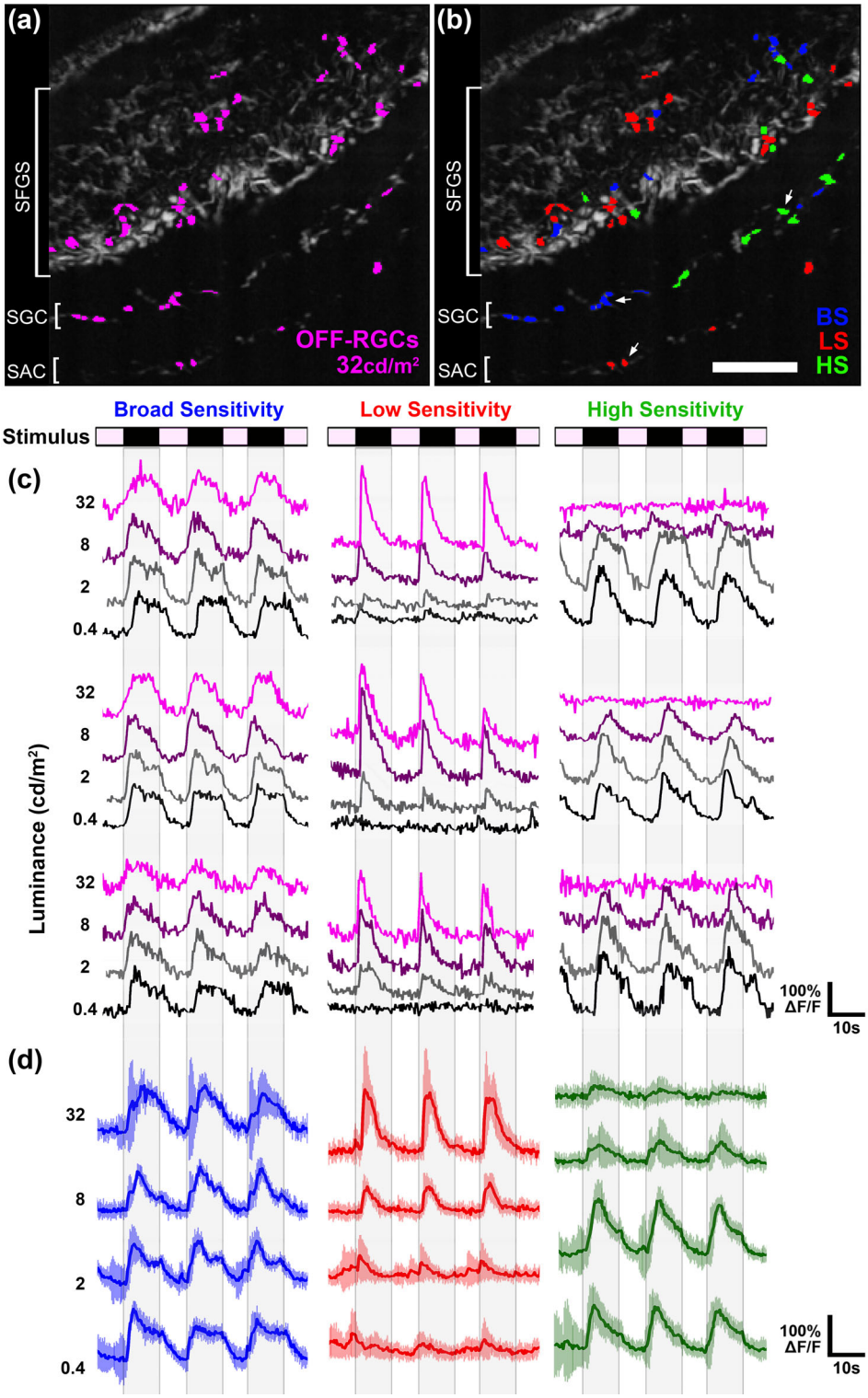

FIGURE 4 OFF retinal ganglion cells (OFF-RGCs) are comprised of functional classes with different photosensitivity profiles. (a) Average intensity projection from the left tectum of a 6 dpf *Tg(atoh7:gal4,uas:gcamp6s)* larva during presentation of 32 cd/m^2 dimming stimulus to the right eye. Dimming detector regions of interest (ROIs) identified by cross-correlation based image segmentation are shown in magenta. (b) Image in (a) with ROI color coding that indicates photosensitivity profile of individual OFF-RGC terminals. BS (broad sensitivity) ROIs in blue correspond to OFF-RGC terminals that responded strongly to trials at all stimulus intensities (0.4, 2, 8, and 32 cd/m^2). LS (low sensitivity) ROIs in red correspond to OFF-RGC terminals that responded optimally to trials with high light intensities during the ON phase (>8 cd/m^2). HS (high sensitivity) ROIs in green correspond to OFF-RGC terminals that responded optimally to trials with low light intensities during the ON phase (>8 cd/m^2). (c) Sample traces of individual BS, LS, and HS OFF-RGC terminals in tectum shown in (a and b). Each trace is 58 s in duration and consists of four ON phases of 7-s duration interleaved with three OFF phases of 10-s duration. The BS OFF-RGC responds robustly at all stimulus intensities. In contrast, the LS OFF-RGC did not respond at low light intensities, whereas the HS OFF-RGC did not respond at high light intensities. (d) Average intensity traces of BS, LS, and HS OFF-RGC terminals in the tectum shown in (a and b) (n = 11 ROIs for each group). Error bars represent SD. Scale bar: 20 μm in (a and b)

arbors that stratify in specific tectal layers (Del Bene et al., 2010; Gabriel et al., 2012; Robles et al., 2011; Scott & Baier, 2009), these response type-specific differences in layer innervation could provide an anatomical basis by which OFF-RGC inputs with specific photosensitivities could activate distinct tectal circuits. Consistent with this possibility, *id2b:gal4*-positive TLPNs form dendrites that arborize in SFGS5/6 and SGC layers of tectum (DeMarco et al., 2019), which are innervated by a large fraction of HS OFF-RGCs terminals.

3.4 | The optic tectum contains dimming-responsive neurons with different photosensitivity profiles

The zebrafish optic tectum is the largest visual brain area and receives direct input from 97% of all RGCs (Robles et al., 2014). Furthermore, tectal circuitry has been shown to play a crucial role in both attractive and aversive visually guided behaviors (Barker &

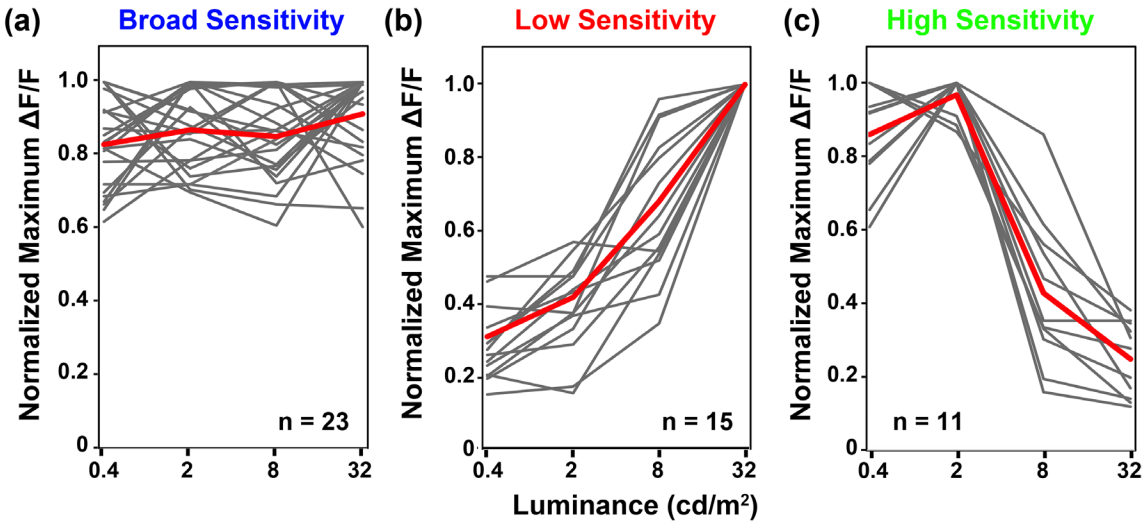

FIGURE 5 (a–c) Photosensitivity tuning curves for OFF retinal ganglion cells (OFF-RGCs) detected in tectum of larva used in Figure 4. Individual region of interest (ROI) responses are shown in gray, average of these traces is shown in red. Data are presented as peak ΔF/F normalized to the maximum value for each RGC ROI in any of the trials. Data represents 59 ROIs detected in three larvae. Note diversity of responses within each functional class

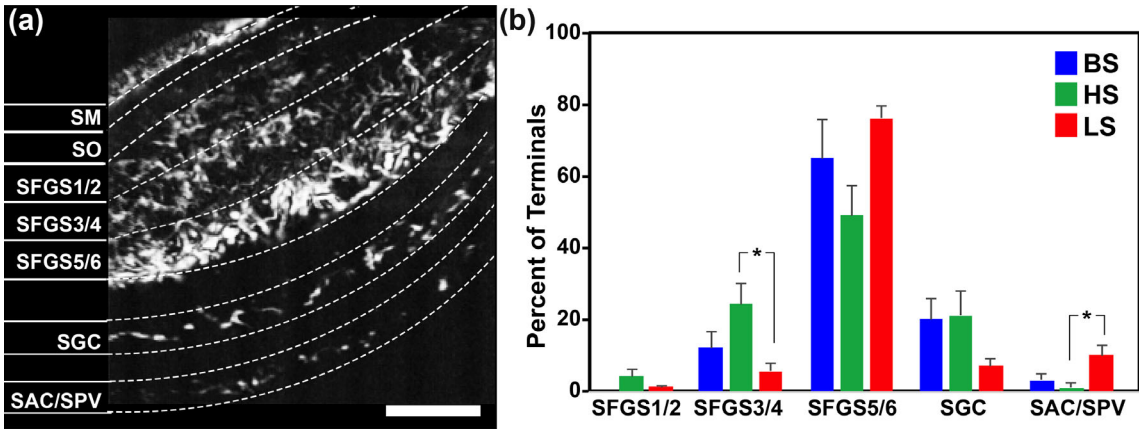

FIGURE 6 Layer-specific innervation of tectum by broad sensitivity, high sensitivity, and low sensitivity OFF retinal ganglion cell (OFF-RGC) terminals. (a) Average intensity projection of a recording from the tectum of a *Tg(atoh7:gal4,uas:gcamp6s)* double transgenic larva during stimulus presentation. Overlaid are sublayer boundaries used for tectal sublayer designations. (b) Distribution of OFF-RGC classes by tectal neuropil sublayer. Data represents 290 regions of interest detected in eight larvae. Scale bar: 20 μm

Baier, 2015; Dunn et al., 2016; Helmbrecht, Dal Maschio, Donovan, Koutsouli, & Baier, 2018; Temizer et al., 2015). To examine the response properties of tectal neurons to the same dimming stimuli used to distinguish OFF-RGC subclasses, we performed two-photon calcium imaging in the optic tectum of *Tg(Elavl3:Gal4-VP16)* × *Tg(14xUAS-GCAMP6S)* transgenic larvae, in which GCaMP6s is expressed in nearly all neurons (Figure 7a). The cross-correlation-based image segmentation approach used for RGCs was similarly applied to identify tectal neurons that responded to the same dimming protocol (ON light intensities of 0.4, 2, 8, and 32 cd/m^2). While dimming-responsive neurons were identified in all tecta imaged, these neurons were a small minority of all cells, representing 5.4 ± 0.9% of tectal neurons (Figure 7b; *n* of 10 tecta). Consistent with a model in which OFF-RGC classes activate distinct brain circuits, we identified subsets of dimming-responsive neurons in the tectum with photosensitivity profiles similar to those observed in OFF-RGCs (Figure 7c). Notably, BS, HS, and LS tectal neuron response types were present in similar proportions (37.8 ± 3.6%, 36.4 ± 2.6%, and 25.8 ± 4%, respectively; Figure 7d), and all three were located throughout the anteroposterior extent of the tectum (Figure 7b). We cannot confirm that BS dimming-responsive tectal neurons inherit their photosensitivity profiles from BS OFF-RGC axons; some or all may integrate inputs from both HS and LS OFF-RGCs. However, the presence of HS and LS tectal neurons indicates that these tectal neuron subpopulations most likely receive synaptic input selectively from HS and LS OFF-RGCs, respectively. It should

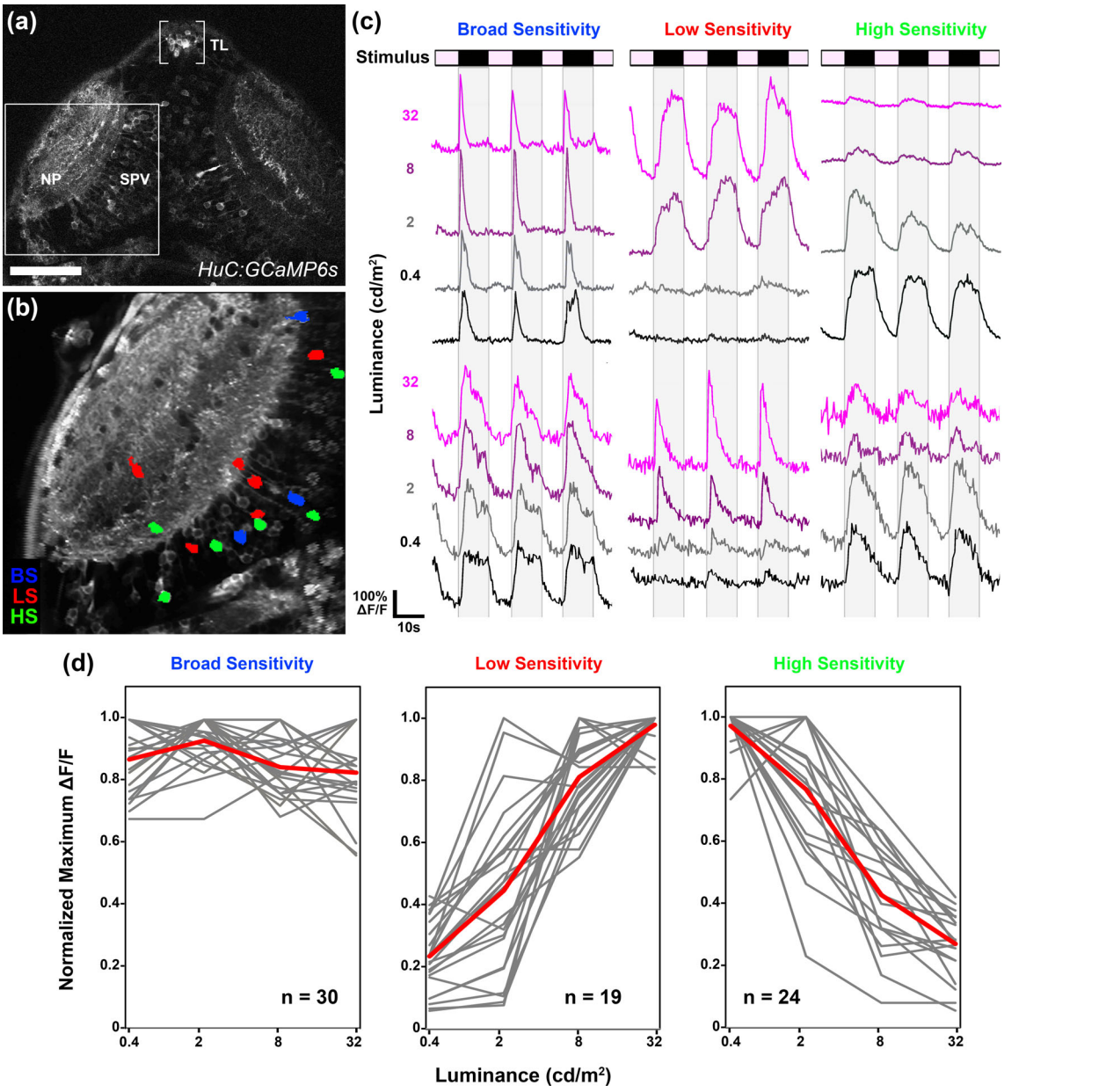

FIGURE 7 Optic tectum contains dimming-responsive neurons with different photosensitivities. (a) Low-magnification dorsal view of a 6 dpf *Tg(Elavl3:gal4,uas:gcamp6s)* larva. Boxed region indicates typical field of view used for functional imaging trials. (b) Average intensity projection from a recording in the left tectum of a 6 dpf *Tg(elavl3:gal4,uas:gcamp6s)* larva presented with light steps to the right eye. Region of interest color coding indicates photosensitivity profile of dimming-responsive tectal neurons: broad sensitivity (BS; blue), low sensitivity (LS; red), and high sensitivity (HS; green). Note sparse and dispersed distributions of neurons in both the neuropil (NP) and periventricular (SPV) layers of the tectum. (c) Sample traces of individual BS, LS, and HS tectal neurons. Each trace is 58 s in duration and consists of four ON phases of 7-s duration interleaved with three OFF phases of 10-s duration. (d) Photosensitivity tuning curves for 73 dimming-responsive neurons (BS, LS, and HS) detected in 10 tecta (gray). Average of individual traces is shown in red. Scale bar: 80 μm in (a), 40 μm in (b)

also be noted that the tuning of tectal dimming responses exhibited a high degree of variability, similar to the responses we observed in TLPNs (compare Figure 1h and Figure 7d). These findings confirm segregation of HS and LS dimming channels at the first stage of visual processing in the brain, where they activate distinct tectal circuits.

3.5 | TL contains dimming-responsive neurons with distinct photosensitivity profiles

In ray-finned fish, the TL is a visual brain structure reciprocally connected to the optic tectum that does not receive direct retinal input (Gibbs & Northmore, 1996; Northmore, 2017). We examined

neuronal responses in the TL of *Tg(Elavl3:Gal4-VP16)* × *Tg(14xUAS-GCAMP6S)* larvae presented with the same dimming stimulus series used to identify OFF-RGCs and dimming-responsive tectal neurons. Consistent with previous reports in other teleost species, we find that the larval zebrafish TL contains dimming-responsive neurons (Northmore, 1984). Unlike in tectum, where such neurons were rare, a large percentage of neurons in both TL lobes responded to light intensity decreases (57.8 ± 8.6%; Figure 6b,c; n = 5 larvae). Similar to our findings in the optic tectum, we found TL also contained dimming responsive neurons with BS, HS, and LS photosensitivity profiles (Figure 6d-g). Notably, neurons exhibiting these three response types were also present in similar proportions in TL (BS = 34.4 ± 5.6%; HS = 28.9 ± 4.5%; BS = 36.7 ± 1.1%, respectively). The presence of dimming responsive neurons with different photosensitivities suggests that the TL may play a general role in processing light level information, as previously proposed (Gibbs & Northmore, 1996). However, the existence of HS and LS neurons in TL is consistent with a model in which high- and low-intensity dimming information remains segregated across three distinct stages of visual processing: retina, tectum, and TL. Our data suggest that *id2b:gal4*-positive TLPNs transmit HS dimming information to specific subsets of dimming-responsive neurons in TL, while BS and LS dimming information may be transmitted to TL by TLPNs that are never or rarely (see Figure 1h) labeled by the *id2b:gal4* transgene.

4 | DISCUSSION

Combining cell type-specific genetic labeling with in vivo functional imaging allowed us to identify dimming-responsive neurons across three levels of sensory processing in retina, tectum and TL. These findings demonstrated that BS, HS, and LS dimming pathways remain segregated in the brain. Although ON and OFF signals are known to be processed separately in the mammalian visual pathway (Komban et al., 2014), few visual circuits in the brain have been identified that respond preferentially to either larger or small dimming steps. This may reflect an experimental bias originating from observations that neuronal response properties in primate visual cortex are not strongly influenced by light levels (Duffy & Hubel, 2007). Brain imaging in humans support these findings, as presentation of scotopic and photopic stimuli activates similar brain regions, with the exception of regions specialized for color vision, which do not receive rod-derived information (Hadjikhani & Tootell, 2000). However, there is evidence that subcortical circuits in mammals contain units that respond in a light level-dependent manner, including neurons in the suprachiasmatic nucleus (Meijer, Groos, & Rusak, 1986), pretectum (Clarke & Ikeda, 1985), and superior colliculus (Stein, Labos, & Kruger, 1973). Our findings identify specialized circuits in the zebrafish brain for processing light decrements of different amplitudes.

Functional characterization of retinal inputs to the larval tectum identified OFF-RGC terminals and further demonstrated that these inputs exhibit a wide range of photosensitivity profiles. In the mammalian retina, OFF-RGC output pathways with distinct photosensitivities are thought to be generated by contributions from separate rod- and cone-driven retinal circuits (Völgyi et al., 2004). in vivo optical recordings of synaptic transmission in the larval zebrafish retina have revealed the existence of bipolar cells with a range of photosensitivity profiles (Odermatt et al., 2012), indicating that parallel dimming-responsive channels can be generated in the retina upstream of RGCs. Although we cannot exclude contributions from the small number of rods present at the periphery of the larval zebrafish retina (Zimmermann et al., 2018), it is unclear if these are functional photoreceptors at this age (Bilotta et al., 2001). Given that diverse responses were observed using stimuli in the mesopic–photopic range, we consider it likely that a separate photosensing mechanism contributes to "tuning" responses to light-intensity ranges within the broad operating range of cones. It has previously been proposed that wide-field amacrine cells that provide modulatory input to bipolar cell terminals could be activated at different light levels than individual cone bipolar cells (Odermatt et al., 2012). Presynaptic inhibition of bipolar cell terminals by amacrine cells with narrow photosensitivity profiles could provide a means to tune OFF-RGC responses, thus generating HS and/or LS responses. An alternative explanation is that the diversity of OFF-RGC responses elicited by our broad-spectrum stimulus display is due to cone types that signal over different ranges of light intensity. Indeed, recent experimental evidence has demonstrated that zebrafish cone types differ in both their sensitivities and saturation thresholds (Nelson, Balraj, Suresh, Torvund, & Patterson, 2019). Within this model, HS and LS dimming responses in the brain (RGC axons, tecum, and TL) could arise through RGC pathways that convey information derived from cone channels that are differentially activated and saturated by the light steps we employed. In this scenario, RGCs identified as BS, LS, and HS channels in response to broad-spectrum stimuli may also encode wavelength information (i.e., color). Although direct evidence for color-specific RGC channels in the larval zebrafish is currently lacking, there is anatomical and functional data suggesting that highly UV-sensitive RGC channels likely exist in ventral retina (Zimmermann et al., 2018). Regardless of the retinal mechanism generating different OFF responses, it is clear that stereotyped visual behaviors in zebrafish larvae are evoked to similar extents by both broad-spectrum and wavelength-specific stimuli (optomotor response; Orger & Baier, 2005; and visual motor response; Burton, Zhou, Bai, & Burton, 2017). Therefore, it stands to reason that wavelength-specific information converges upstream of the brain circuits that control these behaviors.

Our data also identified a genetically specified tectum–TL pathway specialized to transmit HS dimming information. The HS dimming pathway could be essential for spatial navigation and body axis orientation in fish species that occupy complex, poorly lit environments. Consistent with this model, the TL is highly developed in reef fish (Ito & Kishida, 1978), which occupy complex photoenvironments and often engage in nocturnal foraging (Horodysky, Brill, Crawford, Seagroves, & Johnson, 2013). Based on the diversity of photosensitivities observed in dimming-responsive TL neurons, the larval tectum likely also contains

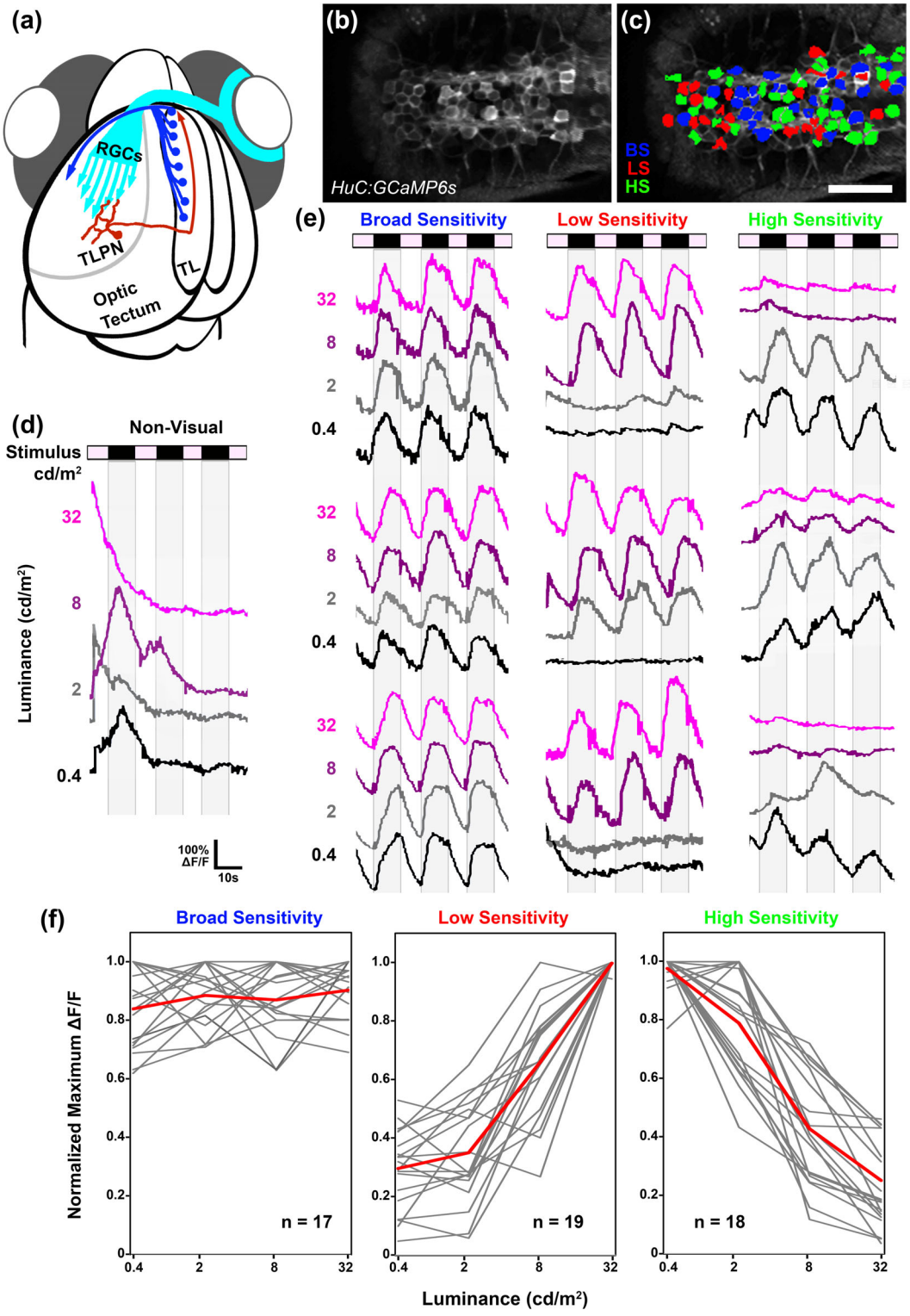

FIGURE 8 Parallel dimming pathways remain segregated in torus longitudinalis (TL). (a) Schematic of retinal ganglion cell innervation of the tectum and reciprocal connection between the tectum and TL. (b) Single multiphoton image from a recording in the TL of a 6 dpf *Tg(elavl3:gal4,uas:gcamp6s)* larva presented with light steps to the right eye. Anterior is to the right. (c) Region of interest color coding indicates photosensitivity profile of individual TL neurons: broad sensitivity (BS; blue), low sensitivity (LS; red), and high sensitivity (HS; green). Note dense activation of many neurons on both sides of the TL. Anterior is to the right. (d) Sample trace of a nonvisual TL neuron. Note large events that are highly variable with respect to stimulus timing across trials. (e) Sample traces of individual BS, LS, and HS TL neurons. Each trace is 58 s in duration and consists of four ON phases of 7-s duration interleaved with three OFF phases of 10-s duration. Note that in several traces, baseline drifted in either the positive or negative direction. (f) Photosensitivity tuning curves for 54 dimming-responsive neurons detected in TL (gray). Average of individual traces is shown in red. Scale bar: 40 μm

genetically distinct BS and LS TLPN subtypes that form parallel dimming pathways to TL. Based on the response of TL neurons to changes in light levels in the contralateral visual field, it has been proposed that this area could play a specific role in the processing of interocular light-level differences (Northmore, 1984b). The TL also contributes to the dorsal light reflex (DLR), an innate behavior where adult fish tilt their body axis to orient their dorsal aspect toward a light source, equalizing both the amount of light hitting each eye and the gravitational forces measured by the vestibular system on each side (Gibbs & Northmore, 1996). In addition to the DLR, calculation of interocular light level differences could also be used by the visual system to assist in tracking objects as they move from one visual hemifield to the other (Northmore, 2017). In this scenario, activation of one tectal lobe by a moving stimulus would transmit a priming signal to the opposite lobe that could function to heighten its detection sensitivity in anticipation of the stimulus entering its visual hemifield. The TL could serve such a function based on the fact that regions of TL receive input from both tectal lobes (DeMarco et al., 2019) and a whole-field dimming stimulus presented to one eye activates neurons in both contralateral and ipsilateral lobes of TL (see Figure 8). Further experimentation will be required to test the hypothesis that TL input to tectum regulates circuits involved in prey detection and tracking.

ACKNOWLEDGMENTS

The authors thank A. Chubykin and A. Pak for assistance with data analysis, and D. Suter, E. Fernandez-Juricic, Y-F. Leung, M. Fernandes, D. Mearns, and E. DeMarco for comments on the manuscript. Funding was provided by the Max Planck Society (H.B. and E.R.) and the Purdue Institute for Integrative Neuroscience (E.R.).

CONFLICT OF INTEREST

The authors declare no potential conflict of interest.

AUTHOR CONTRIBUTIONS

E.R. and H.B. conceived the experiments and wrote the paper; E.R. and N.P.F. performed the experiments and analysis.

DATA AVAILABILITY STATEMENT

The raw data supporting the conclusions of this manuscript will be made available by the authors, without undue reservation, to any qualified researcher.

ORCID

Estuardo Robles https://orcid.org/0000-0002-1202-2050

REFERENCES

Antinucci, P., Suleyman, O., Monfries, C., & Hindges, R. (2016). Neural mechanisms generating orientation selectivity in the retina. *Current Biology: CB*, *26*, 1802–1815.

Barker, A. J., & Baier, H. (2015). Sensorimotor decision making in the zebrafish tectum. *Current Biology: CB*, *25*, 2804–2814.

Bilotta, J., Saszik, S., & Sutherland, S. E. (2001). Rod contributions to the electroretinogram of the dark-adapted developing zebrafish. *Developmental Dynamics*, *222*, 564–570.

Burton, C. E., Zhou, Y., Bai, Q., & Burton, E. A. (2017). Spectral properties of the zebrafish visual motor response. *Neuroscience Letters*, *646*, 62–67.

Clarke, R. J., & Ikeda, H. (1985). Luminance and darkness detectors in the olivary and posterior pretectal nuclei and their relationship to the pupillary light reflex in the rat. *Experimental Brain Research*, *57*, 224–232.

Cook, P. B., & McReynolds, J. S. (1998). Lateral inhibition in the inner retina is important for spatial tuning of ganglion cells. *Nature Neuroscience*, *1*, 714–719.

Del Bene, F., Wyart, C., Robles, E., Tran, A., Looger, L., Scott, E. K., … Baier, H. (2010). Filtering of visual information in the tectum by an identified neural circuit. *Science*, *330*, 669–673.

DeMarco, E., Xu, N., Baier, H., & Robles, E. (2019). Neuron types in the zebrafish optic tectum labeled by an id2b transgene. *The Journal of Comparative Neurology*, *528*(7), 1173–1188.

Duffy, K. R., & Hubel, D. H. (2007). Receptive field properties of neurons in the primary visual cortex under photopic and scotopic lighting conditions. *Vision Research*, *47*, 2569–2574.

Dunn, T. W., Gebhardt, C., Naumann, E. A., Riegler, C., Ahrens, M. B., Engert, F., & Del Bene, F. (2016). Neural circuits underlying visually evoked escapes in larval Zebrafish. *Neuron*, *89*, 613–628.

Fleisch, V. C., & Neuhauss, S. C. F. (2006). Visual behavior in zebrafish. *Zebrafish*, *3*, 191–201.

Gabriel, J. P., Trivedi, C. A., Maurer, C. M., Ryu, S., & Bollmann, J. H. (2012). Layer-specific targeting of direction-selective neurons in the zebrafish optic tectum. *Neuron*, *76*, 1147–1160.

Gibbs, M. A., & Northmore, D. P. M. (1996). The role of torus longitudinalis in equilibrium orientation measured with the dorsal light reflex. *Brain, Behavior and Evolution*, *48*, 115–120.

Hadjikhani, N., & Tootell, R. B. (2000). Projection of rods and cones within human visual cortex. *Human Brain Mapping*, *9*, 55–63.

Helmbrecht, T. O., Dal Maschio, M., Donovan, J. C., Koutsouli, S., & Baier, H. (2018). Topography of a visuomotor transformation. *Neuron*, *100*, 1429–1445.e4.

Horodysky, A. Z., Brill, R. W., Crawford, K. C., Seagroves, E. S., & Johnson, A. K. (2013). Comparative visual ecophysiology of mid-Atlantic temperate reef fishes. *Biology Open*, *2*, 1371–1381.

Ito, H., & Kishida, R. (1978). Afferent and efferent fiber connections of the carp torus longitudinalis. *The Journal of Comparative Neurology*, *181*, 465–475.

Komban, S. J., Kremkow, J., Jin, J., Wang, Y., Lashgari, R., Li, X., … Alonso, J.-M. (2014). Neuronal and perceptual differences in the temporal processing of darks and lights. *Neuron*, *82*, 224–234.

Kramer, A., Wu, Y., Baier, H., & Kubo, F. (2019). Neuronal architecture of a visual center that processes optic flow. *Neuron*, *103*, 118–132.e7.

Meijer, J. H., Groos, G. A., & Rusak, B. (1986). Luminance coding in a circadian pacemaker: The suprachiasmatic nucleus of the rat and the hamster. *Brain Research*, *382*, 109–118.

Meyer Zum Alten Borgloh, S. (2015). CalciumSignalExtract: A Matlab GUI to automatically extract the activity of multiple cells from calcium imaging data. Gilbert Laboratory. https://digitalcommons.rockefeller.edu/gilbert_laboratory/2.

Nelson, R. F., Balraj, A., Suresh, T., Torvund, M., & Patterson, S. S. (2019). Strain variations in cone wavelength peaks in situ during zebrafish development. *Visual Neuroscience*, *36*, E010 https://www.cambridge.org/core/journals/visual-neuroscience/article/strain-variations-in-cone-wavelength-peaks-in-situ-during-zebrafish-development/27191946AF02B01C37FF6ED3CD3DF797

Nikolaou, N., Lowe, A. S., Walker, A. S., Abbas, F., Hunter, P. R., Thompson, I. D., & Meyer, M. P. (2012). Parametric functional maps of visual inputs to the tectum. *Neuron*, *76*, 317–324.

Northmore, D. P. M. (1984). Visual and saccadic activity in the goldfish torus longitudinalis. *Journal of Comparative Physiology A*, *155*, 333–340.

Northmore, D. P. M. (2017). Holding visual attention for 400 million years: A model of tectum and torus longitudinalis in teleost fishes. *Vision Research*, *131*, 44–56.

Odermatt, B., Nikolaev, A., & Lagnado, L. (2012). Encoding of luminance and contrast by linear and nonlinear synapses in the retina. *Neuron*, *73*, 758–773.

Orger, M. B., & Baier, H. (2005). Channeling of red and green cone inputs to the zebrafish optomotor response. *Visual Neuroscience*, *22*, 275–281.

Pérez-Schuster, V., Kulkarni, A., Nouvian, M., Romano, S. A., Lygdas, K., Jouary, A., … Sumbre, G. (2016). Sustained rhythmic brain activity underlies visual motion perception in Zebrafish. *Cell Reports*, *17*, 1098–1112.

Pologruto, T. A., Sabatini, B. L., & Svoboda, K. (2003). ScanImage: Flexible software for operating laser scanning microscopes. *Biomedical Engineering Online*, *2*, 13.

Portugues, R., & Engert, F. (2009). The neural basis of visual behaviors in the larval zebrafish. *Current Opinion in Neurobiology*, *19*, 644–647.

Ratliff, C. P., Borghuis, B. G., Kao, Y.-H., Sterling, P., & Balasubramanian, V. (2010). Retina is structured to process an excess of darkness in natural scenes. *Proceedings of the National Academy of Sciences*, *107*, 17368–17373.

Robles, E., Filosa, A., & Baier, H. (2013). Precise lamination of retinal axons generates multiple parallel input pathways in the tectum. *Journal of Neuroscience: The Official Journal of the Society for Neuroscience*, *33*, 5027–5039.

Robles, E., Laurell, E., & Baier, H. (2014). The retinal Projectome reveals brain-area-specific visual representations generated by ganglion cell diversity. *Current Biology*, *24*, 2085–2096.

Robles, E., Smith, S. J., & Baier, H. (2011). Characterization of genetically targeted neuron types in the zebrafish optic tectum. *Frontiers in Neural Circuits*, *5*, 1.

Scott, E. K., & Baier, H. (2009). The cellular architecture of the larval zebrafish tectum, as revealed by gal4 enhancer trap lines. *Frontiers in Neural Circuits*, *3*, 13.

Semmelhack, J. L., Donovan, J. C., Thiele, T. R., Kuehn, E., Laurell, E., & Baier, H. (2014). A dedicated visual pathway for prey detection in larval zebrafish. *eLife*, *3*, e04878.

Stein, B. E., Labos, E., & Kruger, L. (1973). Determinants of response latency in neurons of superior colliculus in kittens. *Journal of Neurophysiology*, *36*, 680–689.

Straw, A. D. (2008). Vision egg: An open-source library for realtime visual stimulus generation. *Frontiers in Neuroinformatics*, *2*, 4.

Temizer, I., Donovan, J. C., Baier, H., & Semmelhack, J. L. (2015). A visual pathway for looming-evoked escape in larval Zebrafish. *Current Biology: CB*, *25*, 1823–1834.

Völgyi, B., Deans, M. R., Paul, D. L., & Bloomfield, S. A. (2004). Convergence and segregation of the multiple rod pathways in mammalian retina. *Journal of Neuroscience: The Official Journal of the Society for Neuroscience*, *24*, 11182–11192.

Xiao, T., & Baier, H. (2007). Lamina-specific axonal projections in the zebrafish tectum require the type IV collagen dragnet. *Nature Neuroscience*, *10*, 1529–1537.

Xiao, T., Staub, W., Robles, E., Gosse, N. J., Cole, G. J., & Baier, H. (2011). Assembly of lamina-specific neuronal connections by slit bound to type IV collagen. *Cell*, *146*, 164–176.

Zimmermann, M. J. Y., Nevala, N. E., Yoshimatsu, T., Osorio, D., Nilsson, D.-E., Berens, P., & Baden, T. (2018). Zebrafish differentially process color across visual space to match natural scenes. *Current Biology: CB*, *28*, 2018–2032. e5.

How to cite this article: Robles E, Fields NP, Baier H. The zebrafish visual system transmits dimming information via multiple segregated pathways. *J Comp Neurol*. 2021;529: 539–552. https://doi.org/10.1002/cne.24964